An AlGaN/GaN HEMT with enhanced breakdown and a near-zero breakdown voltage temperature coefficient*

Xie Gang(谢 刚)[a)b)], Tang Cen(汤 岑)[a)], Wang Tao(汪 涛)[a)],
Guo Qing(郭 清)[a)], Zhang Bo(张 波)[c)], Sheng Kuang(盛 况)[a)†], and Wai Tung Ng[b)]

[a)] *College of Electrical Engineering, Zhejiang University, Hangzhou* 310027, *China*
[b)] *The Edward S. Rogers Sr. Electrical and Computer Engineering Department, University of Toronto, Toronto, Ontario, Canada, M5S 1A1*
[c)] *State Key Laboratory of Electronic Thin Films and Integrated Devices, University of Electronic Science and Technology of China, Chengdu* 610054, *China*

(Received 16 August 2012; revised manuscript received 10 September 2012)

An AlGaN/GaN high-electron mobility transistor (HEMT) with a novel source-connected air-bridge field plate (AFP) is experimentally verified. The device features a metal field plate that jumps from the source over the gate region and lands between the gate and drain. When compared to a similar size HEMT device with a conventional field plate (CFP) structure, the AFP not only minimizes the parasitic gate to source capacitance, but also exhibits higher OFF-state breakdown voltage and one order of magnitude lower drain leakage current. In a device with a gate to drain distance of 6 μm and a gate length of 0.8 μm, three times higher forward blocking voltage of 375 V was obtained at $V_{GS} = -5$ V. In contrast, a similar sized HEMT with a CFP can only achieve a breakdown voltage no higher than 125 V using this process, regardless of device dimensions. Moreover, a temperature coefficient of 0 V/K for the breakdown voltage is observed. However, devices without a field plate (no FP) and with an optimized conventional field plate (CFP) exhibit breakdown voltage temperature coefficients of −0.113 V/K and −0.065 V/K, respectively.

Keywords: AlGaN/GaN high-electron mobility transistor, air-bridge field plate, breakdown voltage, breakdown voltage temperature coefficient

PACS: 61.72.uj, 71.20.N, 51.50.+v **DOI:** 10.1088/1674-1056/22/2/026103

1. Introduction

AlGaN/GaN heterojunction high electron mobility transistors (HEMTs) have been under extensive investigation because of their projected superb performance as high power switching devices,[1–11] including low on-resistance, high breakdown voltage (BV), and high temperature operation. In order to fully develop the potential of HEMTs and suppress the current collapse effect, it is important to suppress the drain side gate edge electric field strength.[12,13] Recent work has placed emphasis on improving the OFF-state blocking capability without introducing process complexity and parasitics. Field plate (FP) structures have been shown to be effective in enhancing the breakdown voltage and reducing C_{gd} for silicon power devices.[14] However, for commercially RF process, only a limited breakdown voltage improvement can be obtained with conventional FP structures due to the undesirable thickness of the SiN passivation (e.g., 150 nm). Based on such a thin SiN passivation thickness, the FP is less effective. Boutros *et al.*[15] fabricated an HEMT with a source FP length of 0.7 μm which can provide a breakdown voltage of only 200 V. In addition, the source-connected FP structure reduces C_{gd}, but at the cost of a slight increase in C_{gs}, especially for long gate length.[16]

On the other hand, a negative temperature coefficient of the breakdown voltage is one of the main hindrances to putting the devices into real high power/high temperature applications. Temperature related breakdown behavior has been studied by many groups. Kotani *et al.* attributed the negative temperature coefficient of breakdown voltage to electron hopping at the AlGaN surface.[17] However, our recent investigation suggested that the negative breakdown voltage temperature coefficient is mainly attributed to the native or generated traps/defects gate tunneling and electric field induced hot electron injection from the gate metal to the channel.[18]

In this paper, a novel source-connected air-bridge field plate (AFP) is introduced to achieve high breakdown voltage even with a very thin SiN passivation of 150 nm in an RF process. HEMT devices with a conventional source-connected FP over an SiN layer of the same thickness were also fabricated for comparison purpose. Fabrication results indicated that the proposed air-bridge devices exhibit a 3× improvement in OFF-state breakdown voltage and show a near-zero breakdown voltage temperature coefficient when compared to devices with CFP and no FP devices.

*Project supported by the Delta Science & Technology Educational Development Program (Grant No. DREK2010001) and the Zhejiang Provincial Natural Science Foundation of China for Distinguished Young Scholars (Grant No. R1100468).

†Corresponding author. E-mail: shengk@zju.edu.cn

© 2013 Chinese Physical Society and IOP Publishing Ltd

2. Device structure and simulation model

Devices with CFP and AFP are shown in Fig. 1, where L_{FP} and L_M are the length of the CFP and the length of air-bridge footprint, respectively. L_{GF} is the distance between the gate edge and the air-bridge footprint. Figure 1(c) shows the SEM view of the fabricated novel AFP HEMT. All the HEMTs with no FP, CFP, and AFP feature the same physical device dimensions. In the simulation, the Al mole fraction in the AlGaN layer was 0.28. The thickness of the SiN passivation layer is 150 nm. A sheet carrier density of 1.1×10^{13} cm^{-2} caused by the piezoelectric and polarization dipole was modeled along the upper side of the AlGaN/GaN interface to define the 2DEG sheet carrier concentration. According to the Chynoweth[19] impact ionization model and Monte Carlo simulation of the impact ionization in wurtzite GaN, the impact ionization model in our simulation is

$$\alpha = \alpha_n^{\infty} \exp\left[-\left(\frac{F_{cn}}{F}\right)^{kn}\right], \quad (1)$$

where α_n^{∞} and F_{cn} are the impact ionization rate and critical electric field for electrons, respectively. The same formula can be obtained for holes. Electron ionization rates and hole ionization rates can be calculated to be 2.6×10^8 cm^{-1} and 4.98×10^6 cm^{-1}, respectively. Critical electric fields for electrons and holes can be calculated to be 3.42×10^7 V/cm and 1.95×10^7 V/cm, respectively, and these were used in the simulation.

Traps with a maximum concentration of 1×10^{14} cm^{-3} and a relative energy level of 1.1 eV were also assigned to model the semi-insulating substrate to suppress parasitic substrate conduction. Electron mobility of 1800 cm$^2 \cdot$V$^{-1} \cdot$S^{-1} was also modeled along the 2DEG channel. Other device parameter values employed for simulation are shown in Table 1.

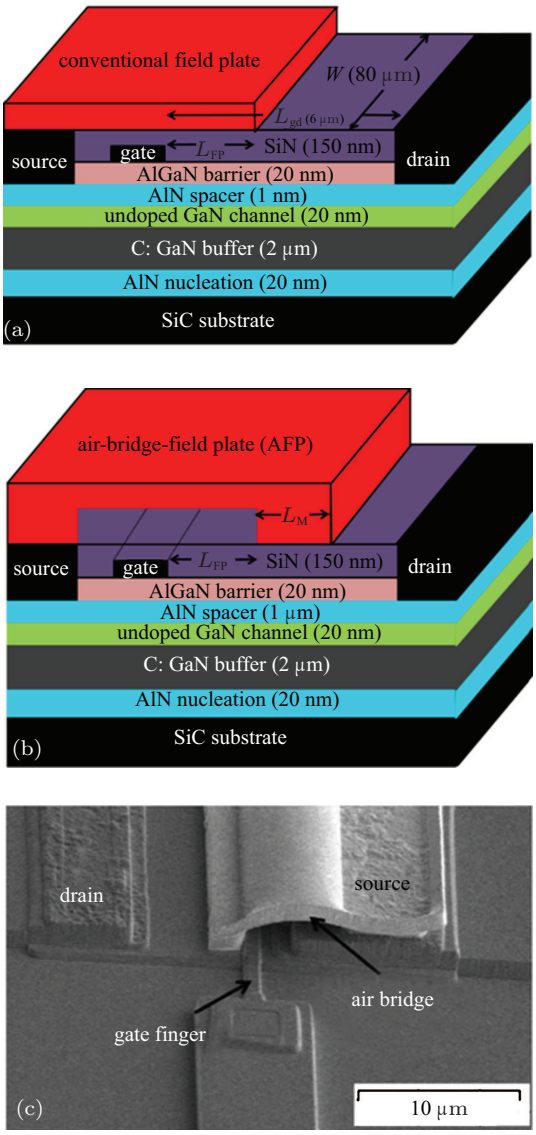


Fig. 1. (color online) Cross-sectional view of the proposed HEMT structure: (a) with a CFP, where L_{FP} is the FP length. (b) AlGaN/GaN HEMT with novel AFP, where L_{GF}, L_M, L_{GD} are the gate-to-air-bridge field plate distance, air-bridge footprint width, and gate-drain distance (drift region), respectively. (c) SEM view of fabricated novel AFP HEMT.

Table 1. Material parameters for simulation.

Parameters	AlGaN	GaN
Bandgap/eV	4.15	3.47
Electron mobility/cm$^2 \cdot$V$^{-1} \cdot$S^{-1}	550	1100
Electron saturation velocity/cm $\cdot$ s^{-1}	1.5×10^7	2.1×10^7

3. Results and discussion

The devices were fabricated on a 3-inch RF GaN-on-SiC process. The epitaxial layer structure consists of an unintentionally doped AlGaN barrier layer (20 nm)/i-AlN spacing layer (1 nm)/i-GaN channel layer (200 nm)/C-doped insulating layer (2 μm)/AlN nucleation layer (20 nm). The Al mole fraction in the AlGaN layer was 0.28. A sheet carrier density of 1.1×10^{13} cm^{-2} and an electron mobility of 1800 cm$^2 \cdot$V$^{-1} \cdot$S^{-1} were obtained by Hall measurements. Transmission line measurement (TLM) indicates that the Ohmic contact resistance varies from 0.52 Ω $\cdot$ mm to 0.67 Ω $\cdot$ mm across the wafer. The device active area was first defined by mesa etching. The Ohmic contact using Ti/Al/Ni/Au (285 nm) was deposited by e-beam evaporation and annealed at 850 °C for 30 s in N_2 ambience. The Schottky gate was formed by an e-beam evaporated Pt-based (430 nm) layer without annealing. This was defined using lift-off processes. A 150-nm plasma-enhanced chemical vapor deposition (PECVD) Si_3N_4 passivation film was deposited followed by a 1000-nm thick layer of Au metallization, which can be used to implement the AFP or CFP. The APF and CFP HEMT on a thin dielectric can be fabricated by the same process at the same time.

Figure 2(a) illustrates the measured C_{gs} as a function of V_{gs} for HEMTs with and without a conventional FP (L_{FP} = 1.2 μm), and an AFP with L_M = 2 μm, L_{GF} = 0.5 μm. Since the dielectric constant of air is 1, the air-bridge HEMT exhibits much lower C_{gs} when compared to the case with a CFP. The OFF-state I–V characteristics of these devices are shown in Fig. 2(b). For the conventional HEMT without an FP, a forward blocking voltage of 37 V was obtained with a drain leakage current of over 10^{-2} A/mm before breakdown occurs with $V_{GS} = -5$ V. The HEMT with a conventional optimized FP (L_{FP} = 1.2 μm) has an improved breakdown voltage of no higher than 125 V. The leakage current was also slightly suppressed. The proposed HEMT with an AFP achieved a forward blocking voltage of 375 V, which is three times higher than the HEMT with a conventional FP. Furthermore, the leakage current for the HEMT with an AFP is one order of magnitude lower when compared to the conventional devices, from 10^{-2} A/mm to around 10^{-3} A/mm.

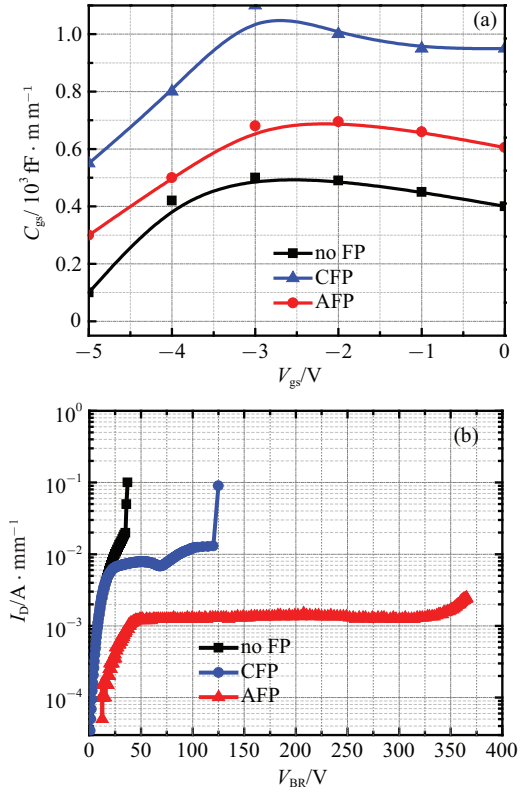


Fig. 2. (color online) (a) Measured C_{gs} as a function of V_{gs}. (b) OFF-state of I–V characteristics of the fabricated AlGaN/GaN HEMTs. The breakdown voltages (actual breakdown point) for devices without an FP, with a CFP, and with the proposed AFP are 37 V, 125 V, and 375 V, respectively. Unless otherwise noted, the devices have the same designed physical dimension, where L_{FP} = 1.2 μm, L_{GS} = 1.1 μm, L_G = 0.8 μm, L_{GF} = 0.5 μm, L_M = 2 μm, and L_{GD} = 6 μm.

APSYS-TCAD[20] device simulations were carried out to illustrate the device concept. In order to provide a fair comparison, CFP and AFP devices with individually optimized dimensions but with the same cell pitch were simulated at the same drain voltage of 240 V. The AFP relies on the air gap to increase the effective thickness of the field dielectric. As illustrated in Fig. 3(a), the surface electric field distribution along the AlGaN/GaN interface for the AFP structure exhibits lower electric field strength near both the drain side gate edge and FP edge. This clearly shows that the devices with an AFP still have room to accommodate higher drain voltage and with lower gate edge electric field induced leakage. Next, CFP and AFP devices with the same equivalent FP dimensions and the same cell pitch were also simulated at near-breakdown conditions ($E = E_c$ = 3.3 MV/cm). The simulated drain voltage of the HEMT with an AFP having L_M = 2 μm, L_{GF} = 0.5 μm is 450 V. The simulated drain voltage for the device with a conventional FP having L_{FP} = 2.5 μm is 235 V. The electric field distributions for HEMTs near breakdown with the same effective FP length are as shown in Fig. 3(b). The low dielectric constant of air can better modulate the surface electric field distribution, allowing the device with an AFP to support higher breakdown voltage even with the same device dimensions.

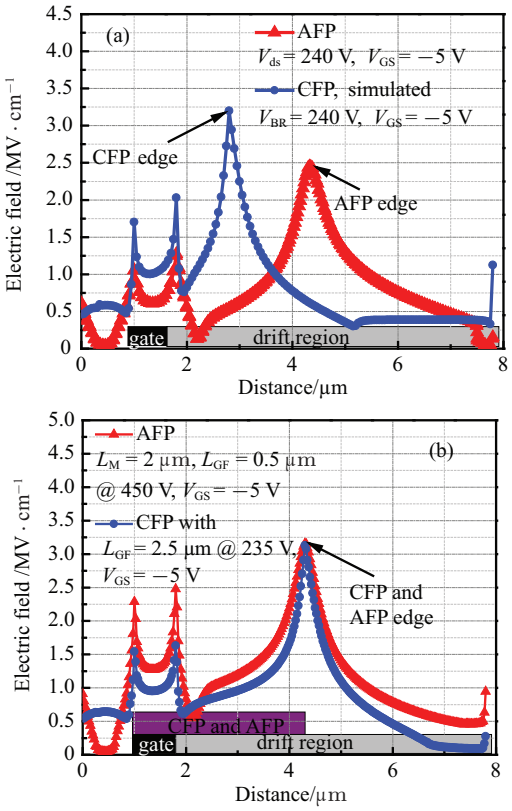


Fig. 3. (color online) (a) Simulated electric field strength of an AFP device with L_M = 2 μm, L_{GF} = 0.5 μm, with the drain applied voltage of V_{ds} = 240 V and a conventional FP device (simulated breakdown voltage $BV_{(s)}$ = 240 V) with L_{FP} = 1.2 μm. The simulated breakdown voltage of the AFP device with L_M = 2 μm, L_{GF} = 0.5 μm is 450 V. (b) Simulated electric field for devices with the same effective FP length ($L_M + L_{GF} = L_{FP}$ = 2.5 μm). Critical electric field E_c is around 3.3 MV/cm. Acceptor and donor like traps (density = 2×10^{16} cm^{-3}, energy level E_t = 0.9 eV) were modeled under the gate of the channel area. Electron and hole ionization rates for the GaN buffer and channel regions were specified as 2.6×10^8 cm^{-1} and 4.98×10^6 cm^{-1}, respectively.

Measured breakdown voltages (V_{BR}) as a function of L_M

with different L_{GF} are shown in Fig. 4(a). Three samples from different wafers were measured. It can be observed that breakdown voltage (2 mA/mm) has the best device dimension tolerance as a function of L_M with $L_{GF} = 0.5$ μm. Breakdown voltage degrades slightly from 375 V for $L_M = 2$ μm, $L_{GF} = 0.5$ μm to 325 V for $L_M = 5$ μm, $L_{GF} = 0.5$ μm. The breakdown voltage degrades dramatically for those devices with L_{GF} above 0.8 μm and L_M above 3 μm. Breakdown voltage also degrades dramatically for those devices with L_{GF} above 0.8 μm and L_M below 2 μm. This can be explained by the fact that the premature breakdown occurs near the drain side when L_{GF} above 0.8 μm, L_M above 3 μm and gate edge when L_{GF} above 0.8 μm, L_M below 2 μm. Breakdown voltage of the device with conventional FP is also shown in Fig. 4(b). The longest L_{FP} fabricated was 3 μm. Breakdown voltage increases from 37 V without FP to 125 V with conventional L_{FP} length of ∼1.2 μm. No further increase in breakdown voltage was observed after this point. Surface electric field distributions for those devices with $L_M = 5$ μm, L_{GF} length from 0.2 μm to 1 μm are shown in Fig. 5.

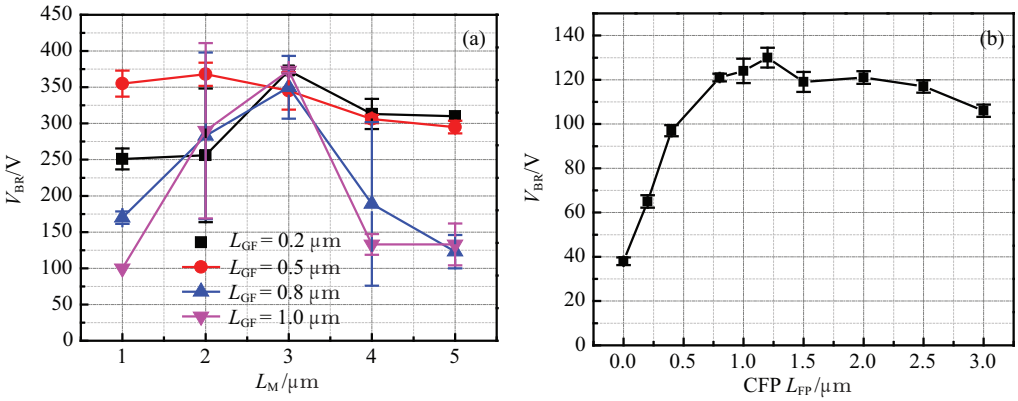


Fig. 4. (color online) (a) Measured breakdown voltage (V_{BR}) as a function of L_M with different L_{GF} for AFP devices and (b) breakdown voltage as a function of convention L_{FP} for CFP devices.

From Fig. 5(a), it can easily be observed that the surface peak electric field moves to the drain side with increasing L_{GF}. Premature breakdown happens near the drain side. From Fig. 4(a), breakdown voltage also degrades dramatically for those devices with $L_M = 1$ μm and, L_{GF} above 0.8 μm. Surface electric field distributions for those devices are shown in Fig. 5(b) to help understand the possible reasons. As illustrated in Fig. 5(b), the electric field strength near FP edge decreases with increasing L_{GF}, while the peak electric field near the drain side gate edge increases with increasing L_{GF}. This can indicate that the premature breakdown happens near the gate edge.

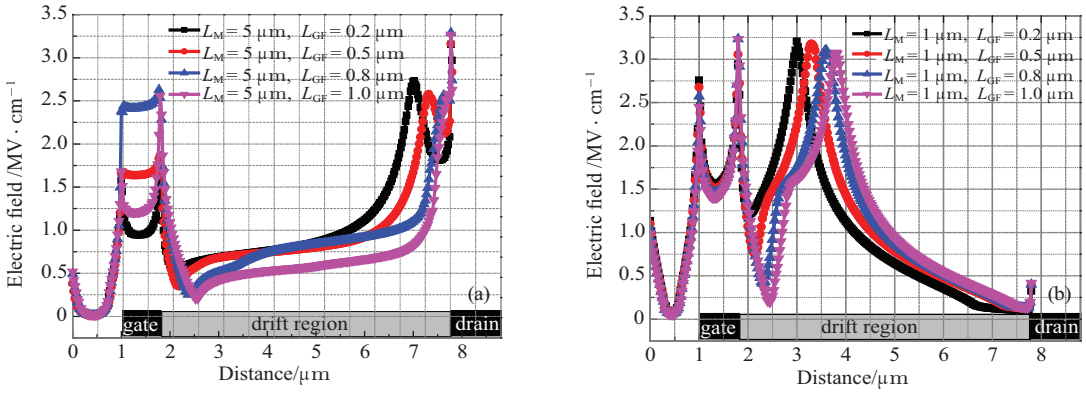


Fig. 5. (color online) (a) Simulated electric field distribution along AlGaN/GaN interface as a function of L_{GF}, where $L_M = 5$ μm. (b) Simulated electric field distribution along AlGaN/GaN interface as a function of L_{GF}, where $L_M = 1$ μm.

Figure 6(a) illustrates the measured breakdown voltage with different temperatures. As we can see from this figure, breakdown voltage remains almost constant with increasing temperature. A near-zero temperature coefficient for the breakdown voltage is observed from room temperature (RT) to 400 K. This can be explained in that the AFP can suppress the drain side gate edge electric field induced gate to channel injection.[18] However, as the temperature is further increased to 450 K, the breakdown voltage decreases from 350 V to 320 V. The Schottky gate leakage current increases and starts to dominate at elevated temperatures. As illustrated in Fig. 6(b), the breakdown voltage temperature coefficients for HEMTs with and without an FP were measured to be −0.065 V/K and −0.113 V/K, respectively.[18]

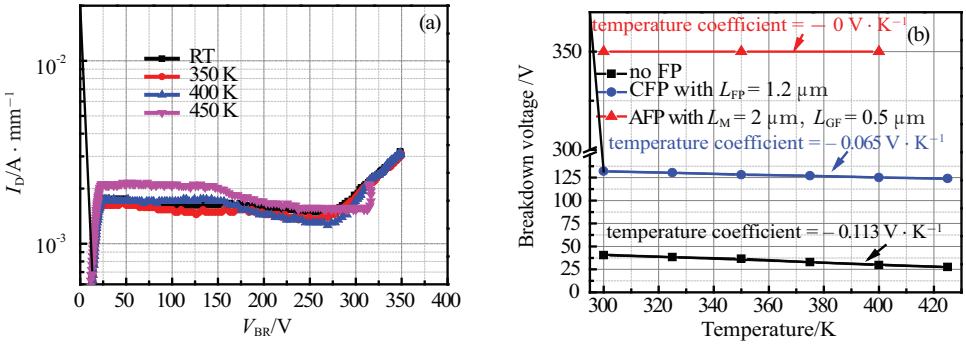


Fig. 6. (color online) Measured breakdown voltage with different temperatures for (a) HEMT with an AFP, (b) temperature coefficient of breakdown voltage for conventional HEMT (no FP), HEMT with CFP, HEMT with the novel AFP, respectively.

4. Conclusion

An AlGaN/GaN HEMT featuring a novel AFP has been experimentally verified. When compared to HEMTs with a conventional FP, a 3× higher breakdown voltage and one order of magnitude lower drain leakage current is obtained via layout changes only. High electric field hot carrier injection is reduced. A near-zero breakdown voltage temperature coefficient is obtained via layout changes only for temperatures ranging from RT to 400 K. The fabrication process for the AFP HEMT is fully compatible with the commercial RF GaN technology without the need for any additional photolithography or processing steps.

References

[1] Ibbetson J P, Fini P T, Ness K D, DenBaars S P, Speck J S and Mishra U K 2000 *Appl. Phys. Lett.* **77** 250
[2] Nanjo T, Takeuchi M, Suita M, Oishi T, Abe Y, Tokuda Y and Aoyagi Y 2008 *Appl. Phys. Lett.* **92** 263
[3] Zhang J F, Mao W, Zhang J C and Hao Y 2008 *Chin. Phys.* B **17** 689
[4] Guo B Z, Gong N and Yu F Q 2008 *Chin. Phys.* B **17** 290
[5] Wang M J and Chen K J 2011 *IEEE Trans. Electron Dev.* **58** 460
[6] Wang X D, Hu W D, Chen X S and Lu W 2012 *IEEE Trans. Electron. Dev.* **59** 1393
[7] Xue J S, Zhang J C, Hou Y W, Zhou H, Zhang J F and Hao Y 2012 *Appl. Phys. Lett.* **100** 013507
[8] Hu W D, Chen X S, Quan Z J, Xia C S, Lu W and Ye P D 2006 *J. Appl. Phys.* **100** 074501
[9] Meng F N, Zhang J C, Zhou H, Ma J C, Xue J S, Dang L S, Zhang L X, Lu M, Ai S, Li X G and Hao Y 2012 *J. Appl. Phys.* **112** 023707
[10] Hu W D, Chen X S, Quan Z J, Zhang X M, Huang Y, Xia C S and Lu W 2007 *J. Appl. Phys.* **102** 034502
[11] Zhang J C, Dong Z D, Qin X X, Zheng P T, Liu L J and Hao Y 2009 *Acta Phys. Sin.* **58** 1959 (in Chinese)
[12] Hong S K, Shim K H and Yang J W 2008 *Electron. Lett.* **44** 1091
[13] Xu C, Wang J, Chen H, Xu F, Dong Z, Hao Y and Wen C P 2007 *IEEE Electron. Dev. Lett.* **28** 942
[14] Xu S M, Korec J, Jauregui D, Kocon C, Molly S, Lin H, Daum G, Perelli S, Barry K, Pearce C, Lopez O and Herbsommer J 2009 *IEDM*, Baltimore, MD, USA, p. 145
[15] Boutros K S, Chandrasekaran S, Luo W B and Mehrotra V 2006 *ISPSD*, June 4–8, Naples, Italy, p. 1
[16] Balzan M L, Drinkwine M J and Winslow T A 2008 *CS MANTECH Conference*, April 14–17, Chicago, lllinois, USA, p. 1
[17] Kotani J, Tajima M, Kasai S and Hashizume T 2007 *Appl. Phys. Lett.* **91** 093501
[18] Xie G, Xu E, Zhang B and Ng W T 2012 *Microelectronics Reliab.* **52** 964
[19] Chynoweth A G 1958 *Phys. Rev.* **109** 1537
[20] www.crosslight.com/applications/HEMT.shtml